Taking apart the two-dimensional infrared vibrational echo spectra: More information and elimination of distortions

Kyungwon Kwak, Daniel E. Rosenfeld, and M. D. Fayer[a)]
Department of Chemistry, Stanford University, Stanford, California 94305, USA

(Received 19 March 2008; accepted 22 April 2008; published online 23 May 2008)

Ultrafast two-dimensional infrared (2D-IR) vibrational echo spectroscopy can probe the fast structural evolution of molecular systems under thermal equilibrium conditions. Structural dynamics are tracked by observing the time evolution of the 2D-IR spectrum, which is caused by frequency fluctuations of vibrational mode(s) excited during the experiment. However, there are a variety of effects that can produce line shape distortions and prevent the correct determination of the frequency-frequency correlation function (FFCF), which describes the frequency fluctuations and connects the experimental observables to a molecular level depiction of dynamics. In addition, it can be useful to analyze different parts of the 2D spectrum to determine if dynamics are different for subensembles of molecules that have different initial absorption frequencies in the inhomogeneously broadened absorption line. Here, an important extension to a theoretical method for extraction of the FFCF from 2D-IR spectra is described. The experimental observable is the center line slope ($\mathrm{CLS}\omega_m$) of the 2D-IR spectrum. The $\mathrm{CLS}\omega_m$ is obtained by taking slices through the 2D spectrum parallel to the detection frequency axis (ω_m). Each slice is a spectrum. The slope of the line connecting the frequencies of the maxima of the sliced spectra is the $\mathrm{CLS}\omega_m$. The change in slope of the $\mathrm{CLS}\omega_m$ as a function of time is directly related to the FFCF and can be used to obtain the complete FFCF. $\mathrm{CLS}\omega_m$ is immune to line shape distortions caused by destructive interference between bands arising from vibrational echo emission, from the 0-1 vibrational transition (positive), and from the 1-2 vibrational transition (negative) in the 2D-IR spectrum. The immunity to the destructive interference enables the $\mathrm{CLS}\omega_m$ method to compare different parts of the bands as well as comparing the 0-1 and 1-2 bands. Also, line shape distortions caused by solvent background absorption and finite pulse durations do not affect the determination of the FFCF with the $\mathrm{CLS}\omega_m$ method. The $\mathrm{CLS}\omega_m$ can also provide information on the cross correlation between frequency fluctuations of the 0-1 and 1-2 vibrational transitions. © *2008 American Institute of Physics*. [DOI: 10.1063/1.2927906]

I. INTRODUCTION

Ultrafast two-dimensional infrared (2D-IR) vibrational echo spectroscopy is a rapidly developing tool for studying fast structural dynamics under thermal equilibrium conditions in condensed matter systems.[1,2] 2D-IR vibrational echo experiments have been successfully applied to study the hydrogen bonding network evolution in water[3–5] and alcohol oligomers,[6] the equilibrium dynamics of aqueous and membrane bound proteins,[7–11] fast chemical exchange and isomerization,[12–14] intramolecular vibrational energy relaxation,[15] and dynamical solute-solvent interactions.[16–18]

In a 2D-IR vibrational echo experiment, three ultrafast mid-IR pulses tuned to the vibrational frequency of interest impinge on the sample. The delay times of the pulses are controlled, and their interactions with the vibrational oscillators generate a third-order polarization in the sample, the vibrational echo, which is emitted in the phase matched direction. The vibrational echo pulse is combined with another mid-IR pulse [the local oscillator (LO)] for heterodyne detection, which provides phase information and amplifies the signal. The combined vibrational echo and LO pulse is frequency resolved using a monochromator. The time between the first pulse and second pulse τ is called the first coherence period. The time between the second and third pulse T_w is called the population time because the second pulse takes molecules from the coherent superposition states produced by the first pulse to a population state, either in the 0 or in the 1 vibrational levels. The third pulse again excites the molecules into a coherent superposition state of either the 0-1 vibrational levels or the 1-2 vibrational levels. The oscillating electric dipole generated during the final coherence period emits the vibrational echo in the phase matched direction.[19]

Qualitatively, the measurement of dynamics with 2D-IR vibrational echo spectroscopy can be understood in the following manner. During the first coherence period, the molecules are labeled with their initial frequencies. Microscopic molecular events can cause the frequency-labeled molecules to evolve to different frequencies during T_w. In the second coherence period, the final frequencies are read out. The 2D spectrum is composed of the initial frequencies of molecules along a horizontal axis, the ω_τ axis, and the final frequencies along a vertical axis, the ω_m axis. A set of 2D spectra is

[a)]Electronic mail: fayer@stanford.edu.

measured as a function of T_w. The frequency evolution of the molecular oscillators (spectral diffusion) during the T_w period causes the shape of the 2D spectrum to change as T_w is increased. The amplitude, position, and peak shape of the 2D spectra provide detailed information on molecular dynamics and structure.[2,7] Line shape analysis is difficult to perform. Even in simple cases, like the determination of the linewidth of a linear IR spectrum, different fitting functions can produce different linewidths.

Spectral diffusion dynamics of the molecular systems can be quantified with the frequency-frequency correlation function (FFCF).[20–26] The FFCF is a key to understanding the structural evolution of molecular systems in terms of amplitudes and time scales of the dynamics. The FFCF is the joint probability distribution that the frequency has a certain initial value at $t=0$ and another value at a later time t. The FFCF connects the experimental observables to the underlying dynamics. Once the FFCF is known, all linear and nonlinear optical experimental observables can be calculated by time-dependent diagrammatic perturbation theory.[21]

The approach most directly related to the underlying theory for the analysis 2D-IR vibrational echo spectra is to apply a global fitting routine to extract the FFCF. The global fitting is done by fitting the multiple T_w dependent 2D-IR spectra and the linear spectrum using the nonlinear and linear response functions. The functional form of the FFCF is assumed. Fluctuation amplitudes and time constants are used as fitting variables. A full response function calculation is performed to obtain the 2D and linear spectra. These are compared to the data, and the parameters in the FFCF are iterated to obtain the best fit. The complexity of this method and the questionable convergence to the global minimum of such multivariable nonlinear fitting has led to searches for observables that are sensitive to the FFCF but do not require the full fitting procedure. A variety of methods have been used with limited success to characterize and extract the FFCF of 2D spectra. These include nodal plane slope,[27–29] ellipticity,[30–33] and dynamic linewidth.[24] None of these methods is wholly satisfactory. The dynamic linewidth and ellipticity can be strongly influenced by the destructive interference between the positive going 0-1 band and the negative going 1-2 band. Both of these methods require determining the linewidths of cuts through the 2D spectrum. Both methods can be used, in principle, to examine dynamics in different portions of the absorption line, but the methods abilities are limited by interference between the two bands. The nodal plane slope uses the interference of the 0-1 and 1-2 bands in the 2D spectrum. However, this nodal plane cannot be defined when the anharmonic shift is too large, and it cannot be used to analyze dynamics that may be distinct in different parts of the spectrum. The slope of the phase spectrum has been shown to be proportional to the FFCF.[30,34] However, the relationship between the observable and the FFCF is satisfied only at the center frequency, making it difficult to compare the dynamics of unresolved subensembles.

Recently, a new method for determining the FFCF from 2D-IR vibrational echo spectra was introduced[35] and applied to a number of systems.[10,11,26] It was shown that the FFCF is directly related to the *inverse* of the slope of the line that connects the peak frequencies of spectra obtained by taking slices parallel to ω_τ for a range of ω_m. We will refer to this method as CLSω_τ because the slices are parallel to ω_τ. The peak of a slice spectrum at one ω_m in a 2D spectrum gives one point on the 2D frequency map $(\omega_m, \omega_\tau^*)$, where ω_τ^* is the frequency of the maximum of the slice spectrum for the cut at ω_m. Connecting these maximum points for a range of ω_m generates a line. At short T_w, the line is tilted close to the diagonal line and has a slope of ~ 1. At sufficiently long T_w, spectral diffusion is complete, and the line is vertical. Therefore, the inverse of the slopes of the lines change from ~ 1 to 0 as T_w increases. The details of how to recover the full FFCF including the homogeneous component from 2D and 1D IR spectra have been provided previously.[35] The method only requires the determination of peak positions, which are much easier to measure than linewidths. Furthermore, the CLSω_τ method is not affected by finite pulse durations and other complications that make other methods prone to errors. However, the direct relation between the FFCF and CLSω_τ cannot be guaranteed when destructive interference between the 0-1 and 1-2 bands causes peak position changes as well as line shape distortions in a 2D-IR spectrum.

In this paper, a modification of the CLSω_m method is presented. This method is called the CLSω_m method because slices through the 2D spectrum are taken parallel to the ω_m axis for a range of ω_τ. The points $(\omega_m^*, \omega_\tau)$ are plotted, and they give a center line. The slope of this center line (not the inverse of the slope) varies from ~ 1 to 0 as T_w is increased, and the change in slope is directly related to the FFCF. It is proven that the CLSω_m method is not affected by line shape distortion, which can be caused by peak intensity differences or by the destructive interference between the 0-1 and 1-2 bands. It is numerically demonstrated that peak shape distortion caused by background absorption does not affect the determination of the FFCF. The CLSω_m method can also be used to investigate possible differences in the dephasing of in the 0-1 and 1-2 bands. Piryatinski and Skinner have shown that the initial slope of the frequency resolved echo peak shift is proportional to the cross correlation function between 0-1 and 1-2 transition frequencies when the 1-2 signal is analyzed.[36] However, there has been no report of how this cross correlation function can be directly obtained from the 2D-IR vibrational echo spectra. Here, we prove that the CLSω_m of the 1-2 band is proportional to the cross correlation function when the anharmonicity is sufficiently large relative to the IR linewidth.

II. THEORETICAL DEVELOPMENT

A. The 2D line shape function in the short time approximation

A 2D-IR vibrational echo line shape function can be derived using a two dimensional Fourier transform of the third order response functions about the two coherence periods. Within the Condon and cumulant approximation, the line shape function of the linear IR and 2D-IR spectra can be described using one common line shape function, $g(t)$.[21] A linear IR spectrum includes only the autocorrelation function between the fundamental transition frequencies because only

the transition between the ground state and first excited state is probed. This is also true for the positive going band in the 2D-IR spectrum. The equivalent of ground state bleaching and stimulated emission contribute to this band and only involve the 0-1 transition between the ground state and the first excited state. As a result, the line shape of this positive band can be described using the autocorrelation function of the 0-1 transition frequencies. In contrast, the negative going band that arises from vibrational echo emission at the 1-2 transition frequency (equivalent to excited state absorption) involves the transition between the first excited state and second excited state (1-2) as well as that between the ground state and first excited state (0-1).[37]

To develop a tractable analytical equation for a 2D-IR spectrum, the short time approximation for each coherence period was applied and a simplified 2D-IR line shape equation including spectral diffusion is employed. This approach has been used previously.[27,30,35] Here, we will use the short time approximate 2D-IR line shape equation to prove the direct proportionality between the CLSω_m and the FFCF. Also, we will show that the CLSω_m is not affected by cancellation of the positive 0-1 transition band by the negative 1-2 transition band within the harmonic approximation. The method for dealing with this problem is very similar to that used to develop the CLSω_τ method. Many of the details have been presented previously.[35] Following the previous approach, the 2D-IR line shape function is

$$R(\omega_m,\omega_\tau)=\frac{4\pi}{\sqrt{C_1(0)^2-C_1(T_w)^2}}\exp\left(-\frac{C_1(0)\omega_m^2-2C_1(T_w)\omega_m\omega_\tau+C_1(0)\omega_\tau^2}{2\sqrt{C_1(0)^2-C_1(T_w)^2}}\right)-\frac{2\pi s^2}{\sqrt{C_1(0)C_3(0)-C_2(T_w)^2}}$$
$$\times\exp\left(-\frac{C_1(0)(\omega_m+\Delta)^2-2C_2(T_w)(\omega_m+\Delta)\omega_\tau+C_3(0)\omega_\tau^2}{2\sqrt{C_1(0)C_3(0)-C_2(T_w)^2}}\right). \quad (1)$$

Here, Δ is the anharmonicity (the difference in frequency between the 0-1 and 1-2 transitions) and s is μ_{21}/μ_{10}, where μ_{ij} is the transition dipole matrix element for the two transitions. s is $\sqrt{2}$ in the harmonic approximation (harmonic oscillator) and is generally $\sim\sqrt{2}$. Three different correlation functions are defined as

$$C_1(t)=\langle\delta\omega_{1,0}(\tau_1)\delta\omega_{1,0}(0)\rangle, \quad (2a)$$

$$C_2(t)=\langle\delta\omega_{2,1}(\tau_1)\delta\omega_{1,0}(0)\rangle, \quad (2b)$$

$$C_3(t)=\langle\delta\omega_{2,1}(\tau_1)\delta\omega_{2,1}(0)\rangle. \quad (2c)$$

The two terms for the 0-1 and 1-2 transitions in the response functions cannot be separated because destructive interference must be included to provide an actual description of the 2D-IR signal. In the previous development of CLSω_τ, only one of the three terms was considered because we assumed there was little effect from interference.

B. The ω_m center line slope for a weakly anharmonic system

In the previous work, two points in the 2D frequency space were chosen to calculate the slope of the line that they define. The points (ω_m,ω_τ^*) were calculated by setting the partial derivative of response function to zero at two fixed ω_m points. Here, we derive the equivalent relationship more generally by not assuming that a straight line connects the maxima. The goal of the derivation is to calculate a general form for the slope of the curve connecting the maxima of the spectral slices, $d\omega_m^*/d\omega_\tau$. This slope can be directly calculated by first setting the partial derivative of the response function to zero, $\partial R(\omega_m,\omega_\tau)/\partial\omega_m=F(\omega_m,\omega_\tau)=0$ at $\omega_m=\omega_m^*$. The equation $F(\omega_m,\omega_\tau)=0$ defines ω_m^* as an implicit function of ω_τ. Taking the total derivative of $F(\omega_m,\omega_\tau)$ gives the equation for $d\omega_m^*/d\omega_\tau$ through the relation between the total derivative and partial derivative $dF(\omega_m^*,\omega_\tau)/d\omega_\tau=[\partial F(\omega_m^*,\omega_\tau)/\partial\omega_m^*](d\omega_m^*/d\omega_\tau)+\partial F(\omega_m^*,\omega_\tau)/\partial\omega_\tau=0$.

After some simplification,

$$\frac{d\omega_m^*}{d\omega_\tau}=\frac{\dfrac{C_1(0)\{C_1(T_w)-C_2(T_w)\}\omega_\tau+C_1(0)C_1(T_w)\Delta}{(C_1(T_w)\omega_\tau-C_1(0)\omega_m)^2}-D(\omega_\tau,\omega_m,T_w,s)\left[\dfrac{(C_1(T_w)\omega_m-C_1(0)\omega_\tau)}{\sqrt{C_1(0)^2-C_1(T_w)^2}}-\dfrac{(C_2(T_w)(\omega_m+\Delta)-C_3(0)\omega_\tau)}{\sqrt{C_1(0)C_3(0)-C_2(T_w)^2}}\right]}{\dfrac{C_1(0)\{C_1(T_w)-C_2(T_w)\}\omega_m+C_1(0)^2\Delta}{(C_1(T_w)\omega_\tau-C_1(0)\omega_m)^2}+D(\omega_\tau,\omega_m,T_w,s)\left[\dfrac{(C_1(T_w)\omega_\tau-C_1(0)\omega_m)}{\sqrt{C_1(0)^2-C_1(T_w)^2}}-\dfrac{(C_2(T_w)\omega_\tau-C_3(0)(\omega_m+\Delta))}{\sqrt{C_1(0)C_3(0)-C_2(T_w)^2}}\right]}, \quad (3)$$

where $D(\omega_\tau,\omega_m,T_w,s)$ is defined as

$$D(\omega_\tau,\omega_m,T_w,s)=\left(\frac{2\{C_1(0)C_3(0)-C_2(T_w)^2\}}{s^2C_1(0)^2-C_1(T_w)^2}\right)\exp\left(-\frac{C_1(0)\omega_m^2-2C_1(T_w)\omega_m\omega_\tau+C_1(0)\omega_\tau^2}{2\sqrt{C_1(0)^2-C_1(T_w)^2}}\right.$$
$$\left.+\frac{C_1(0)(\omega_m+\Delta)^2-2C_2(T_w)(\omega_m+\Delta)\omega_\tau+C_3(0)\omega_\tau^2}{2\sqrt{C_1(0)C_3(0)-C_2(T_w)^2}}\right). \quad (4)$$

This expression cannot be simplified further, which illustrates that the slope of the maximum points is a complicated function of both frequencies and all variables appearing in the response function. Making the harmonic approximation for the three level system reduces all three correlation functions to a single function.

When all three correlation functions are equal, $C(t)=C_1(t)=C_2(t)=C_3(t)$, the slope becomes the normalized FFCF

$$\frac{\partial\omega_m}{\partial\omega_\tau}=\frac{C(T_w)}{C(0)}. \quad (5)$$

It should be emphasized that this relationship is true after making the single assumption for the correlation functions. The harmonic approximation implies that the dephasing of the 0-1 transition is the same as that for the 1-2 transition, and that $\mu_{21}/\mu_{10}=\sqrt{2}$. In general, this is a good approximation, and all three correlation functions can be taken to be the same.

C. The CLS in nonoverlapping case

For an oscillator with a large anharmonicity, the 0-1 and 1-2 transition bands in a 2D-IR spectrum are well separated. Each peak can be analyzed independently without considering the effect of band overlap. This greatly simplifies the equations for CLSω_τ and CLSω_m because each peak can be treated separately. For CLSω_τ, which uses the slices parallel to ω_τ at specific ω_m, the equation that defines the set of (ω_m,ω_τ^*) will be given for the 0-1 and 1-2 transition peaks. When only the 0-1 or the 1-2 peak is included in the response function, the equation for CLSω_τ using the relation $\partial R(\omega_m,\omega_\tau)/\partial\omega_\tau=0$ is

$$C_1(T)\omega_m-C_1(0)\omega_\tau^*=0$$

or

$$C_2(T_w)(\omega_m+\Delta)-C_3(0)\omega_\tau^*=0, \quad (6)$$

$$d\omega_m/d\omega_\tau^*=\frac{C_1(0)}{C_1(T_w)} \quad (0-1 \text{ transition}), \quad (7)$$

$$d\omega_m/d\omega_\tau^*=\frac{C_3(0)}{C_2(T_w)} \quad (1-2 \text{ transition}). \quad (8)$$

Equation (7) shows that CLSω_τ is proportional to the *inverse* of the normalized correlation function. The same result was shown previously, but here we used a more general method to obtain the CLSω_τ equation. The result also proves that within the cumulant and short time approximation the maximum points are connected by a straight line. The second equation for the 1-2 transition gives new information about the cross correlation function $C_2(T_w)$ normalized by the initial amplitude of autocorrelation function $C_3(0)$. If we neglect any differences in the three correlation functions (harmonic approximation), the 0-1 and 1-2 transitions will have the same information and the CLS for each peak will be identical. However, in the general case, the cross correlation function $C_2(T_w)$ can only be obtained from the vibrational echo spectroscopy. $C_3(0)$ can be estimated from the linear IR linewidth of the 1-2 transitions although this can be experimentally.

CLSω_m, which uses the slices parallel to ω_m at specific ω_τ, has the equivalent equations for the case of nonoverlapping 0-1 and 1-2 bands. Using the relation $\partial R(\omega_m,\omega_\tau)/\partial\omega_m=0$, it is readily shown that,

$$d\omega_m^*/d\omega_\tau=\frac{C_1(T_w)}{C_1(0)} \quad (0-1 \text{ transition}), \quad (9)$$

$$d\omega_m^*/d\omega_\tau=\frac{C_2(T_w)}{C_1(0)} \quad (1-2 \text{ transition}). \quad (10)$$

The CLSω_m for the 0-1 transition is directly proportional to the FFCF. The CLSω_m for the 1-2 transition displays a different relation to the FFCF than CLSω_τ. It is the cross correlation function normalized by the fluctuation amplitude of the autocorrelation function, $C_1(0)$. $C_1(0)$ can be obtained by analyzing the 0-1 transition. Therefore, in principle, $C_2(T_w)$ can be obtained from the CLSω_m. In the original derivation of CLSω_τ, it was shown that the homogeneous component can be determined and errors arising from the short time approximation can be eliminated by employing the linear absorption spectrum in addition to the CLSω_τ data obtained from the 2D spectra.[35] This is also true for the 0-1 transition CLSω_m. We have not found a similar method for the determination of a $C_2(T_w)$. The time constants for the decay of $C_2(T_w)$ can be easily obtained and the relative amplitudes of the components can be found, but corrections for the short time approximation's effect on the amplitude of fast decay components cannot be made. However, as shown below in a model calculation, the errors are small.

III. APPLICATIONS

A. CLSω_m independent of line shape distortion from destructive interference

If the anharmonicity is not large compared to the 2D spectral bandwidths, the 0-1 and 1-2 transitions overlap. Because the two bands have opposite signs, destructive inter-

TABLE I. Input parameter (superscript *in*) for generating 2D and 1D spectra and the results obtained from the CLS ω_m calculations (superscript *ob*).

	T_2 (ps)	Δ_2 (cm^{-1})	τ_2 (ps)	Δ_3 (cm^{-1})	τ_3 (ps)
$C_1^{in}(t)$	0.14	41	0.38	34	1.7
$C_2^{in}(t)$	0.14 (0.45)[a]	43 (0.36)[a]	0.43	34 (0.22)[a]	2.6
$C_1^{ob}(t)$	0.14	42	0.37	33	1.7
$C_2^{ob}(t)$	0.46[a]	0.31[a]	0.41	0.23[a]	2.5

[a]Fraction of normalized amplitude.

ference produces distortions of the band shapes. Numerical simulations were performed to see the effects of destructive interference on the CLSω_m. Two cases will be considered. The first case is when the harmonic approximation applies, that is, the correlation functions in Eqs. (2a)–(2c) are equal. For this example, the FFCF determined for the OD hydroxyl stretching mode of dilute HOD in water will be used.[26] The parameters are listed in Table I. The lifetime and orientational relaxation time were included in the calculations although they have little effect. In the second case treated in Sec. III C below, we will consider the consequences of the dynamics of the 1-2 transition being different from those of the 0-1 transition.

The calculated spectra are shown in Fig. 1. At short T_w (A, 200 fs), the center line connecting the maxima lies close to the diagonal. In the absence of homogeneous broadening, the line would be at 45° and have a slope of 1. At 200 fs, the combination of homogeneous dephasing and spectral diffusion makes the slope less than 1. Panel B is the long time limit. Spectral diffusion is complete, and the center line is parallel to the ω_τ axis. The spectra of the slices at various ω_τ points are shown for short and long T_w in Figs. 1(c) and 1(d). The maximum frequencies of the slice spectra ω_m^* at various ω_τ form the set of points in 2D frequency space as $(\omega_m^*, \omega_\tau)$. Connecting these maximum frequencies, points at multiple ω_τ points forms a line. The solid line shown in Fig. 1(a) is a plot of the frequencies of the positive going peaks (0-1 transition) in Fig. 1(c). Figure 1(d) shows that at long time the peak frequencies of all of the slice spectra are the same, which yields the horizontal line in Fig. 1(b). At long time, all frequencies in the absorption line have been sampled by spectral diffusion, and, therefore, the slice spectra are the same for all ω_τ.

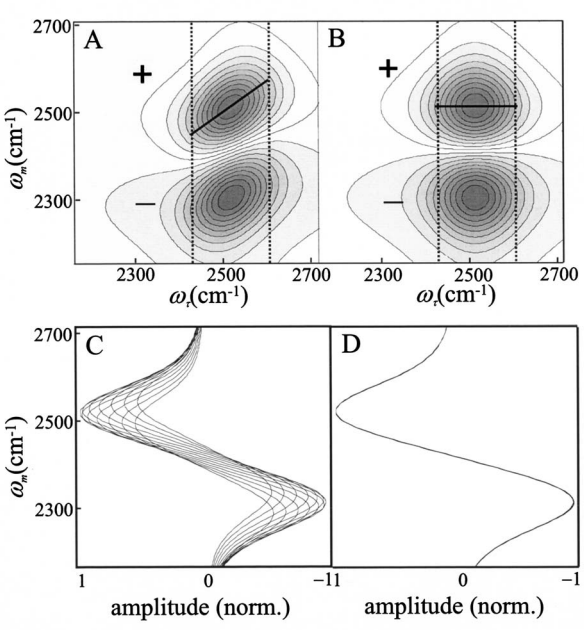

FIG. 1. (A) Calculated 2D-IR vibrational echo spectrum of the OD stretch of HOD/H_2O at T_w=0.2 ps. The parameters used in the calculation are listed in the Table I. (B) Calculated HOD/H_2O 2D-IR spectrum at T_w =5 ps. The heavy lines in (A) and (B) are the center lines. The dotted lines show the range of ω_τ used. (C) and (D) are the projected spectra for (A) and (B) at several ω_m. (C) shows the distribution of peak positions at short T_w. In (D), all of the peak positions are identical which correspond to the horizontal line in (B). To clearly show that all of the slice spectra in (D) have the same maximum position and line shape, each slice spectrum is normalized.

To examine the effect of the overlap of the 0-1 and 1-2 bands on the CLSω_m, the anharmonicity and the transition dipole of the 1-2 transition were varied separately without changing other parameters in the FFCF for the OD stretch of HOD in water used in the calculations. The water 2D-IR spectra at five different anharmonicities and four different s values (ratios of the 0-1 and 1-2 transition dipoles) were calculated. To clearly show the line shape distortion from the change in the anharmonicity and transition dipole, slice spectra along the ω_m axis at T_w=0.2 ps are shown in Figs. 2(a) and 2(b), respectively. As the extent of overlap increases [Fig. 2(a)], the slice spectrum shapes change. In Figs. 2(a) and 2(b), the slice spectra were taken at center frequency of the 0-1 transition, ω_τ=2508 cm^{-1}. If the slice spectra are taken at other ω_τ positions, the spectra will shift to a lower or a higher frequency, depending on the choice of ω_τ. However, the shape changes caused by the overlap display the same trend presented in the figures. The calculated linear IR spectrum with the same parameters has a 160 cm^{-1} full width at half maximum (FWHM). As the anharmonicity becomes small compared to the FWHM, the overlap region becomes increasingly steep, but the line shape on the high frequency side of the 0-1 band (positive going) and the low frequency side of the 1-2 band (negative going) are basically unchanged. s^2 was varied from 1 to 3 with a fixed anharmonicity of 200 cm^{-1}. The slice spectra are shown in Fig. 2(b). The amplitudes have been normalized by the peak intensity of the 0-1 transition. In the harmonic approximation, s^2 is 2, which results in the 0-1 and 1-2 peaks having equal intensities because there are twice as many quantum pathways that contribute to the 0-1 peak than that contribute to the 1-2 peak. In addition to the change in the relative size of the 0-1 and 1-2 bands, the line shape within the overlap region depends on s.

Figures 2(c) and 2(d) show that CLSω_m curves for the

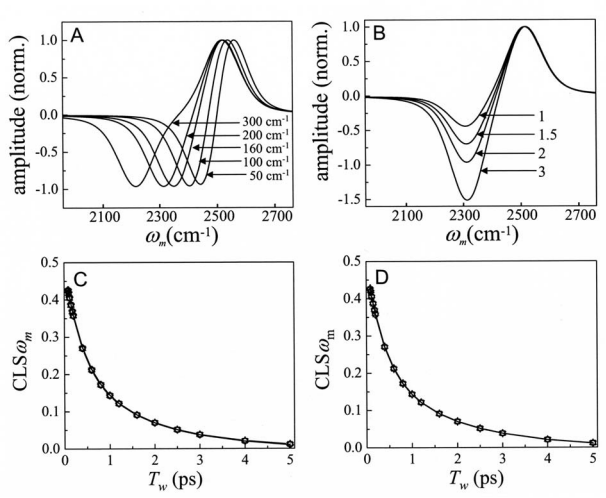

FIG. 2. The effects of the destructive interference between the 0-1 transition positive region of the 2D spectrum and the 1-2 negative region on the CLSω_m determination. (A) The slice spectra at T_w=0.2 ps cut at the ω_τ center frequency of the transition (2508 cm^{-1}) are presented for various anharmonicities: 300, 200, 160, 100, and 50 cm^{-1}. (B) The slice spectra at T_w=0.2 ps cut at the center frequency are presented for various ratios of the transition dipoles squared, s^2: 1, 1.5, 2, 3. All slice spectra are normalized at the maximum intensity of 0-1 peak. (C) CLSω_m curves from each 2D-IR spectrum with different anharmonicities used for A are plotted: 300 cm^{-1} (□), 200 cm^{-1} (○), 160 cm^{-1} (△), 100 cm^{-1} (▽), and 50 cm^{-1} (◇). The points and the curves overlap so well that they cannot be distinguished. (D) CLSω_m curves for various ratios of the transition dipoles squared, s^2: 1 (□), 1.5 (○), 2 (△), 3 (▽). The points and curves overlap so well that they cannot be distinguished.

various anharmonicities (C) and the transition dipole ratios (D). The curves are identical. Although there are five curves in C and four curves in D, they cannot be distinguished from each other. At each point, there are multiple symbols. As proven analytically above, line shape distortions caused by destructive interference do not change the value of the CLSω_m. The CLSω_m curves are directly related to the FFCF. The method for extracting the entire FFCF, including time constants, amplitudes, and the homogeneous component, has been described previously for the CLSω_τ method in detail.[35] However, the CLSω_τ method is susceptible to line shape distortions. Therefore, for systems in which the anharmonicity is not large compared to the FWHM, when using the CLSω_τ method, it is necessary to limit the center lines to the high frequency side of the 0-1 transition where the line shape is not affected by overlap. In contrast, line shape distortions do not affect the CLSω_m and, therefore, do not interfere with the determination of the FFCF.

B. CLSω_m not affected by background absorption

Studies of the effects of high optical density in nonlinear optical experiment have focused on the absorbance of the chromophore under investigation, usually a solute in a liquid or solid solvent.[38–40] The effect of solvent background absorption is generally not considered because the small transition dipole μ of solvent molecules at the wavelength of interest produces a negligible contribution to the third order polarization. The solvent can have a significant absorption due to its high concentration, but because the third order nonlinear signal depends on μ^8 in an intensity level experiment or μ^4 in a heterodyne detected polarization level experiment, the solvent does not contribute to the signal.[41] However, the solvent absorption will reduce the amplitudes of the excitation pulses and reduce the amplitude of the signal pulse as it propagates through the sample. If the solvent background absorption is uniform across the spectrum of the solute peaks of interest, it will have little effect other than reducing the amplitude of the signal. However, in general, the background absorption will not be flat, and it can cause line shape distortions and changes in the relative peak intensities. For example, consider a sample in which the solvent absorbs more strongly on the blue side of the solute spectrum than on the red side. As the vibrational echo propagates through the sample, the blue side of its frequency distribution will be attenuated more than the red side. The excitation pulses will also be attenuated more on the blue side than on the red side, resulting in the generation of more signal on the red side of the spectrum.

The influence of solvent background absorption on the CLSω_m can be separated into the first two excitation pulses, which are associated with the ω_τ axis and the third excitation pulse and the vibrational echo pulse, which are associated with the ω_m axis. Here, we are considering the experimental situation in which the LO pulse that combines with the vibrational echo pulse does not pass through the sample. Therefore, the LO is not changed by the sample absorption.

The first two excitation pulses produce the ω_τ dependent initial population. A nonuniform solvent absorption will distort the initial population along the ω_τ axis. Spectral diffusion will cause this ω_τ frequency-labeled initial population to broaden and move its center frequency. However, the frequency-labeled initial population only evolves along the ω_m axis. Spectral diffusion does not mix populations having different initial excitation frequencies along the ω_τ axis. The frequency dependent absorption of the first two excitation pulses will cause the slice spectra parallel to the ω_m axis to have distortions on their relative amplitudes. Therefore, the 2D spectrum is distorted but the *peak position* of each slice spectrum is not influenced by the distortion of the relative amplitudes of the slices. Thus, the center frequency along the ω_m axis of each slice spectrum is the same in spite of skewing the amount of initial population excited by the first two excitation pulses. As a result, frequency dependent reduction in the first two excitation pulses along ω_τ axis does not affect the CLSω_m.

The effect of nonuniform background on the third excitation pulse and the vibrational echo pulse, which are associated with ω_m, can be described using the IR absorption spectrum. The absorption by the solvent is given by Beer's Law, $I=I(0)e^{-\varepsilon lc}$, where ε is the frequency dependent extinction coefficient, l is the sample thickness, and c is the solvent concentration. The electric field of the third laser pulse becomes $E_3 \propto E_3(0)e^{-\varepsilon lc/2}$. Also, the reduction in the generated echo field can be described in the same way as $E_{\text{echo}} \propto E_{\text{echo}}(0)e^{-\varepsilon lc/2}$. Combining these two frequency dependent absorptions and considering only the ω_m axis, the signal is $S \propto E_L(E_{\text{echo}}(0)E_3(0)e^{-\varepsilon lc})$. E_L is the LO field, which does not pass through the sample. E_1 and E_2 have been omitted because they do not influence the slice spectra along the ω_m

axis. This is an approximate treatment to determine if frequency dependent distortions of the signal caused by the solvent absorption spectrum will influence the determination of the FFCF using the CLSω_m method. The more correct way to do the calculation is to divide the sample into slices and calculate the signal generated in each slice, with the excitation pulses and signal pulse attenuated as they pass through the sample.[42] If the polarization generated by an excitation pulse is sufficiently strong, it needs to be added to the excitation field, which is attenuated in each slice of the sample.[43] In 2D-IR experiments, the polarization generated in the sample is small. Here, we are not attempting to obtain an accurate description of the 2D spectrum as it is distorted by the nonuniform solvent absorption, but rather to see if a distortion influences the CLSω_m method. The simplified approach employed here is sufficient for this purpose.

To determine the effect of nonuniform solvent absorption on the CLSω_m method, 2D-IR vibrational echo spectra with background absorption were calculated. First, the response function without background absorption was calculated using the FFCF of the OD stretch of HOD in water as above. This absorption is centered at 2508 cm^{-1}. As a simple model, the solvent absorption was taken to be a Gaussian function centered at 3000 cm^{-1} with a 1177 cm^{-1} FWHM. This places a large sloping wing under the OD stretch absorption. To simulate the linear IR absorption spectrum with the solvent absorption, the IR spectrum was calculated from the Fourier transform of the linear response function with the same FFCF parameters as used for the 2D-IR calculations discussed above. Then, the model solvent absorption was added to the calculated IR spectrum. As discussed above, the absorption of the first two excitation pulses does not affect the CLSω_m results, so the background absorption was only taken into consideration for the third pulse and the vibrational echo pulse.

To calculate the signal as modified by the background absorption, the spectrum for the vibrational echo emission at the 0-1 and 1-2 transitions was calculated separately. The signal for the 0-1 and 1-2 transitions was reduced according to the amount of absorption in their corresponding frequency ranges, and then the two peaks are combined. The results are shown in Figs. 3(a) and 3(b) for 0.2 and 5 ps, respectively. These two spectra can be compared to Figs. 1(a) and 1(b), which show the 2D-IR spectra without solvent absorption. The shapes are changed and because the solvent absorption is larger in the 0-1 peak region, the 0-1 peak is reduced more than the 1-2 peak, which is evident from number of contours.

Figure 3(c) shows slice spectra along the ω_m axis. The slices are for ω_τ at the center of the spectrum, 2508 cm^{-1}. The absolute value of peaks height for the 0-1 and 1-2 transitions are equal when solvent absorption is not included (solid curve). The solvent absorption is the line in the upper portion of the panel. The inset shows the solvent absorption (line) and the resulting absorption spectrum for the OD stretch and the solvent absorption. The slice spectrum calculated with the solvent absorption is shown in the main part of Fig. 3(c) as the dash and dot curve. Because the background absorption is different across the spectrum, it has a nonuniform effect on the slice spectrum. Both the 0-1 and 1-2 peak

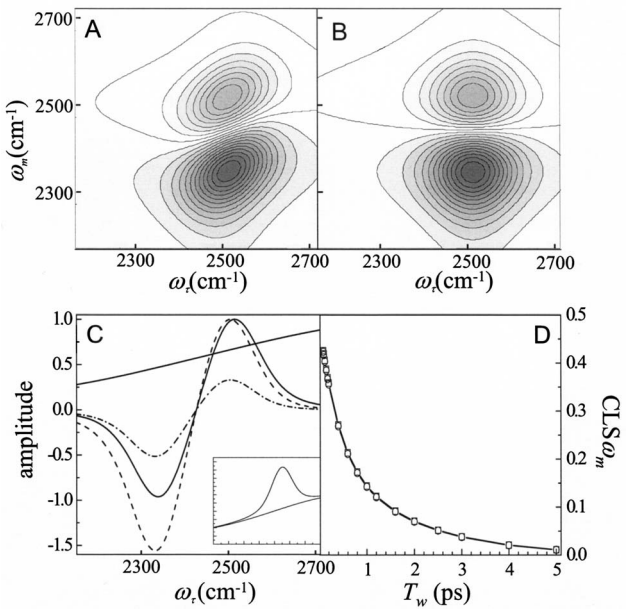

FIG. 3. The effect of solvent background absorption on 2D-IR spectra and CLSω_m determination. (A) Calculated 2D-IR vibrational echo spectrum of the OD stretch of HOD/H_2O at T_w=0.2 ps with solvent absorption. All the parameters for calculating the 2D-IR spectrum are the same as ones used in Fig. 1(a). The model solvent absorption spectrum is shown in Fig. 3(c). (B) Calculated HOD/H_2O 2D-IR spectrum at T_w=5 ps with solvent absorption. The absolute magnitude of 0-1 band is smaller than that of 1-2 band because the solvent spectrum absorption is greater at high frequency. (C) Slice spectra at T_w=0.2 without solvent absorption (solid curve) and with solvent absorption effect (dash and dot curve). For comparison, the 0-1 peak of the slice spectrum with solvent absorption is normalized (dashed curve). The line in the upper part of the panel is the solvent absorption, and the inset shows the solvent absorption (line) and the calculated linear absorption spectrum with the solvent absorption added. (D) CLSω_m curves for the model with solvent absorption (circles) and without solvent absorption (squares). The CLSω_m curves are identical.

amplitudes are reduced, but that of the 1-2 peak is not as reduced as much. To see the difference between the slice spectra with and without the solvent absorption more clearly, the slice spectrum with solvent absorption has been normalized at the peak of the 0-1 transition (dashed curve). The strong solvent absorption at higher frequency pushes the 0-1 peak to a lower frequency and decreases the linewidth. Also, the amplitudes of the 0-1 and 1-2 peaks are very different. CLSω_m were calculated using the simulated spectra with and without solvent absorption and are shown in Fig. 3(d). As is clear from Fig. 3(d), the background solvent absorption does not change the CLSω_m curve and, therefore, will not change the determination of the FFCF in spite of the fact that the 2D spectral shapes are distorted. Fitting of the 2D spectra by using a full response function calculation gives an incorrect determination of the FFCF. The background absorption would have to be included in the calculation. However, using the CLSω_m method, the correct. FFCF will be obtained without considering the spectral distortion induced by solvent absorption.

C. Determining the cross correlation function

As shown in Sec. II A, the 2D-IR signal consists of three different correlation functions [see Eqs. (2a)–(2c)]. Femtosecond mid-IR pulses can have enough bandwidth to excite a

vibrational oscillator from the first to second vibrational excited state; this transition is lower in frequency than the fundamental because of the vibrational anharmonicity. There are open questions as to how the different correlation functions can be studied, if they are significantly different, and theoretical reasons why they should be similar.[36] There has not been a method for extracting the three different correlation functions from a 2D-IR spectrum. Here, we will show that the cross correlation function, $C_2(t)$, between 0-1 and 1-2 transition frequencies can be obtained by analyzing the 1-2 band.

It is possible for the vibrational oscillator dephasing dynamics to be different when it is in the first excited state than in the ground state because of differences in solute-solvent interactions caused by the different bond lengths and dipole moments of the vibrationally excited state. Here, we calculate the 2D-IR spectra including different dynamics for the 0-1 and 1-2 transitions. Therefore, $C_1(t) \neq C_2(t)$ and $C_3(t)$. For these calculations, we use the OD/water FFCF parameters for the 0-1 transition, which determines $C_1(t)$. Different dynamics for the 1-2 transition results in a different $C_3(t)$, the FFCF for the 1-2 transition. There is no simple way to obtain the cross correlation, $C_2(t)$ from the knowledge of $C_1(t)$ and $C_3(t)$. In the calculations, $C_3(t)$ has little effect on the 2D line shapes. It only comes into play during the very brief second coherence period. Therefore, we will simply take $C_2(t)=C_3(t) \neq C_1(t)$. For $C_2(t)=C_3(t)$, we will use the FFCF parameters for the OD stretched of HOD in a 1.5M NaBr aqueous, which are different but not greatly different from those of pure water.[26] These input parameters are given in Table I as $C_1^{\text{in}}(t)$ and $C_2^{\text{in}}(t)$. We also need the lifetime of the second excited state. We use the simple harmonic oscillator result that the second excited state is a factor of 2 faster than the first excited state lifetime.[37] The orientational relaxation is taken to be the same in the 0 and 1 states, and the lifetime and orientational relaxation parameters for pure water are used.[26] The lifetime and the orientational relaxation make very little contribution to the linear or 2D line shape because the homogeneous dephasing T_2 is dominated by the pure dephasing T_2^*.

As a first illustration, the anharmonicity was set to 300 cm^{-1}, which is large compared to the line width of 160 cm^{-1}, to eliminate line shape distortion from overlapping peaks. Below, the influence of the size of the anharmonicity compared to the line width will be considered. The 2D spectra were calculated (see Table I for input parameters), and the linear IR spectrum was also calculated using $C_1^{\text{in}}(t)$. The linear spectrum is used in determining T_2. First, all three correlation functions were set equal, and the 0-1 and 1-2 bands were analyzed separately to check that the analysis of the 0-1 band and the 1-2 band give the same results. The calculated CLSω_m are plotted in Fig. 4(a). The circles show the CLSω_m obtained from the 0-1 transition and the squares are the CLSω_m from the 1-2 band. They overlap well, but close examination reveals that there is a very small difference in the magnitude. This difference comes from the difference in lifetime used for the 2-1 relaxation and the 1-0 relaxation. The lifetime makes a small contribution to the homogeneous component of the FFCF.[35] The homogeneous component manifests itself as the initial difference between the plotted CLSω_m and 1.

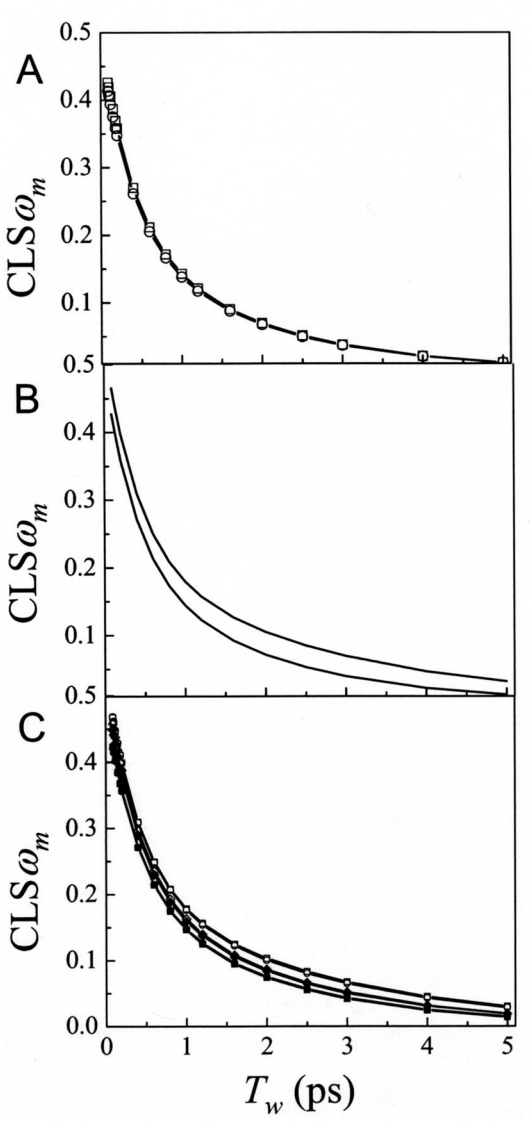

FIG. 4. (A) CLSω_m curves obtained from the 0-1 band (□) and the 1-2 band (○) using the same FFCF for both transitions (OD of HOD in H_2O). The two curves are virtually identical but have a very small difference caused by the faster vibrational decay of second excited state. (B) CLSω_m curves obtained from the 0-1 band (lower curve) and the 1-2 band (upper curve) from the 2D spectra calculated with response function theory using as inputs $C_1(t) \neq C_2(t)$ and $C_3(t)$ (see text). The difference in the curves show that it is in principle possible to obtain $C_2(t)$ as well as $C_1(t)$ using the CLSω_m method. (C) The effect of overlapping peaks in determination of cross correlation function is examined for 2D spectra with $C_1(t) \neq C_2(t)$ and $C_3(t)$ as in (B). The anharmonicity is varied from 200 to 50 cm^{-1} [200 cm^{-1} (□), 160 cm^{-1} (○), and 50 cm^{-1} (◇)]. The closed symbols represent CLSω_m from the 0-1 band and open symbols are for the CLSω_m from 1-2 band. The FWHM of the absorption line width is 160 cm^{-1}. $C_2(t)$ can be obtained as long as the anharmonicity is not small compared to the linewidth.

Figure 4(b) shows the results of the calculations in which $C_1(t) \neq C_2(t)$ and $C_3(t)$. For Fig. 4(b), the anharmonicity is still taken to be 300 cm^{-1}. It is clear from Fig. 4(b) that the CLSω_m obtained from the 0-1 band (lower curve) is distinguishable from that obtained from the 1-2 band (upper curve). The differences in CLSω_ms show that, in principle, both $C_1(t)$ and $C_2(t)$ can be measured.

In Table I, $C_1^{ob}(t)$ and $C_2^{ob}(t)$ obtained from the CLSω_m analysis are compared to the inputs to the 2D response function calculations using $C_1^{in}(t)$ and $C_2^{in}(t)$. In the determination of the 0-1 FFCF from CLSω_m, it is necessary to use the absorption line shape to obtain the absolute FFCF and to determine the homogeneous component.[35] Without use of the absorption line, the FFCF time constants can be determined and the relative fractional amplitudes of the components can be determined, but the absolute values in wave numbers and an accurate T_2 in picoseconds cannot be determined. There is no equivalent of the absorption line to use in conjunction with the determination of $C_2(t)$. Therefore, in Table I for $C_2^{ob}(t)$, the time constants and fractional amplitudes are listed. As can be seen in Table I, the agreement between the input parameters and those obtained from the CLSω_m analysis is very good.

In the calculations presented in Fig. 4(b), the anharmonicity (300 cm^{-1}) is large compared to the linewidth (160 cm^{-1}). Figure 4(c) shows the results of the calculations in which the anharmonicity is varied with all other parameters identical to those used in Fig. 4(b). Three sets of calculations were performed with anharmonicities of 200, 160, and 50 cm^{-1}. The results for 200 and 160 cm^{-1} (as well as 300 cm^{-1}, not shown) are identical. These results are the upper curves obtained from the 1-2 band and the lower curves obtained from the 0-1 band. The two curves in Fig. 4(c) that virtually overlap and are between the upper and lower curves are for 50 cm^{-1} anharmonicity. These cannot be distinguished. The 50 cm^{-1} anharmonicity is less that a third of the line width. The 0-1 and 1-2 bands overlap almost completely. Whether information on $C_2(t)$ can be obtained is dependent on the magnitude of the anharmonicity relative to the line width, not the absolute linewidth. To determine $C_2(t)$, there must be a reasonable degree of separation between the 0-1 and 1-2 bands.

IV. CONCLUDING REMARKS

We have presented a new approach, the CLSω_m method, for extracting the FFCF from 2D-IR vibrational echo spectra. The CLSω_m method is an extension and improvement on the previously described CLSω_τ method.[35] Details of the practical aspects of using the CLSω_m method are the same as in CLSω_τ method and are described in Ref. 35. Here, it was demonstrated that distortions of the 2D line shapes caused by overlap of the positive going 0-1 band and the negative going 1-2 band do not affect the determination of the FFCF using the CLSω_m. This is not the case for the previously detailed CLSω_τ method. Because of the lack of distortion caused by overlapping bands, it is possible to use the CLSω_m method to examine different frequency ranges of a 2D spectrum to determine if the dynamics vary with frequency.[44] Investigation of a frequency dependence can be accomplished by using slice spectra on the blue side of the line and on the red side of the line, and comparing the CLSω_m. If the CLSω_m are different on the two sides of the line, then frequency dependent subensembles that have different dynamics that exist in the molecular system.

It was also demonstrated that the CLSω_m is not sensitive to distortions in the 2D spectra produced by nonuniform background absorption. Frequently, a very weak absorption of interest is riding on top of a large sloping solvent absorption. The solvent does not produce a signal because it has a small transition dipole, but it has significant absorption owing to its high concentration. Large background absorption often occurs in biological samples, where the vibration of interest produces a small absorption on top of very significant water and protein absorptions. Using the CLSω_m method, the FFCF can be accurately obtained in spite of distortions to the 2D spectrum produced by the solvent absorption. It was shown previously that the CLS method, whether CLSω_m or CLSω_τ, yields the correct FFCF even when the 2D spectra are distorted by finite pulse durations or apodization along one axis.[35] In addition, the CLSω_m was shown to be capable of obtaining more information than the 0-1 transition FFCF. The method is also able to obtain the cross correlation function between fluctuations of the 0-1 and 1-2 vibrational transitions.

In addition to the usefulness of the CLSω_m to obtain various types of information without distortion, it is also important for its speed in data analysis and its lack of sensitivity to systematic errors. In contrast to doing full response theory calculations of the 2D and linear spectra to iteratively fit the experimental spectra to obtain the FFCF, the CLSω_m yields the FFCF in a simple and fast set of calculations.[35] The reduction in fitting time can be a factor greater than 100. In the CLSω_m method, it is necessary to determine peak positions rather than linewidths or line shapes. Peak positions are much easier to obtain accurately than linewidths or line shapes. The net result is that the CLSω_m method can provide more information in a manner that is less susceptible to error than other approaches. Therefore, the CLSω_m method increases the utility of ultrafast 2D-IR vibrational echo spectroscopy for the extraction of dynamical information from complex molecular systems.

ACKNOWLEDGMENTS

The authors would like to thank the Air Force Office of Scientific Research (F49620-01-1-0018) for support of this work. Daniel E. Rosenfeld was supported by the Fannie and John Hertz Foundation and a Stanford Graduate Fellowship.

[1] J. Zheng, K. Kwak, and M. D. Fayer, Acc. Chem. Res. **40**, 75 (2007).
[2] R. M. Hochstrasser, Adv. Chem. Phys. **132**, 1 (2006).
[3] J. B. Asbury, T. Steinel, K. Kwak, S. Corcelli, C. P. Lawrence, J. L. Skinner, and M. D. Fayer, J. Chem. Phys. **121**, 12431–12446 (2004).
[4] M. L. Cowan, B. D. Bruner, N. Huse, J. R. Dwyer, B. Chugh, E. T. J. Nibbering, T. Elsaesser, and R. J. D. Miller, Nature (London) **434**, 199 (2005).
[5] J. J. Loparo, S. T. Roberts, and A. Tokmakoff, J. Chem. Phys. **125**, 194521 (2006).
[6] J. B. Asbury, T. Steinel, C. Stromberg, K. J. Gaffney, I. R. Piletic, and M. D. Fayer, J. Chem. Phys. **119**, 12981 (2003).
[7] I. J. Finkelstein, J. Zheng, H. Ishikawa, S. Kim, K. Kwak, and M. D. Fayer, Phys. Chem. Chem. Phys. **9**, 1533 (2007).
[8] L. P. DeFlores, Z. Ganim, S. F. Ackley, H. S. Chung, and A. Tokmakoff, J. Phys. Chem. B **110**, 18973 (2006).
[9] P. Mukherjee, I. Kass, I. T. Arkin, and M. T. Zanni, Proc. Natl. Acad. Sci. U.S.A. **103**, 3528 (2006).
[10] H. Ishikawa, I. J. Finkelstein, S. Kim, K. Kwak, J. K. Chung, K. Wakasugi, A. M. Massari, and M. D. Fayer, Proc. Natl. Acad. Sci. U.S.A. **104**, 16116 (2007).

[11] H. Ishikawa, S. Kim, K. Kwak, K. Wakasugi, and M. D. Fayer, Proc. Natl. Acad. Sci. U.S.A. **104**, 19309 (2007).
[12] J. Zheng, K. Kwak, J. B. Asbury, X. Chen, I. Piletic, and M. D. Fayer, Science **309**, 1338 (2005).
[13] Y. S. Kim and R. M. Hochstrasser, Proc. Natl. Acad. Sci. U.S.A. **102**, 11185 (2005).
[14] J. Zheng, K. Kwak, J. Xie, and M. D. Fayer, Science **309**, 1951 (2006).
[15] M. Khalil, N. Demirdoven, and A. Tokmakoff, J. Chem. Phys. **121**, 362 (2004).
[16] J. Wang, J. Chen, and R. M. Hochstrasser, J. Phys. Chem. B **110**, 7545 (2006).
[17] E. C. Fulmer, F. Ding, and M. T. Zanni, J. Chem. Phys. **122**, 034302 (2005).
[18] K. Kwak, S. Park, and M. D. Fayer, Proc. Natl. Acad. Sci. U.S.A. **104**, 14221 (2007).
[19] S. Park, K. Kwak, and M. D. Fayer, Laser Phys. Lett. **4**, 704 (2007).
[20] S. Mukamel, Annu. Rev. Phys. Chem. **51**, 691 (2000).
[21] S. Mukamel, *Principles of Nonlinear Optical Spectroscopy* (Oxford University Press, New York, 1995).
[22] M. Khalil, N. Demirdoven, and A. Tokmakoff, J. Phys. Chem. A **107**, 5258 (2003).
[23] C. J. Fecko, J. J. Loparo, S. T. Roberts, and A. Tokmakoff, J. Chem. Phys. **122**, 054506 (2005).
[24] J. B. Asbury, T. Steinel, K. Kwak, S. A. Corcelli, C. P. Lawrence, J. L. Skinner, and M. D. Fayer, J. Chem. Phys. **121**, 12431 (2004).
[25] J. B. Asbury, T. Steinel, C. Stromberg, S. A. Corcelli, C. P. Lawrence, J. L. Skinner, and M. D. Fayer, J. Phys. Chem. A **108**, 1107 (2004).
[26] S. Park and M. D. Fayer, Proc. Natl. Acad. Sci. U.S.A. **104**, 16731 (2007).
[27] K. Kwac and M. Cho, J. Chem. Phys. **119**, 2256 (2003).
[28] S. Woutersen, R. Pfister, P. Hamm, Y. Mu, D. S. Kosov, and G. Stock, J. Chem. Phys. **117**, 6833 (2002).
[29] J. D. Eaves, J. J. Loparo, C. J. Fecko, S. T. Roberts, A. Tokmakoff, and P. L. Geissler, Annu. Rev. Phys. Chem. **102**, 13019 (2005).
[30] S. T. Roberts, J. J. Loparo, and A. Tokmakoff, J. Chem. Phys. **125**, 084502 (2006).
[31] I. J. Finkelstein, H. Ishikawa, S. Kim, A. M. Massari, and M. D. Fayer, Proc. Natl. Acad. Sci. U.S.A. **104**, 2637 (2007).
[32] C. Fang, J. D. Bauman, K. Das, A. Remorino, E. Arnold, and R. M. Hochstrasser, Proc. Natl. Acad. Sci. U.S.A. **105**, 1472 (2008).
[33] D. Kraemer, M. L. Cowan, A. Paarmann, N. Huse, E. T. J. Nibbering, T. Elsaesser, and R. J. D. Miller, Proc. Natl. Acad. Sci. U.S.A. **105**, 437 (2008).
[34] J. J. Loparo, S. T. Roberts, and A. Tokmakoff, J. Chem. Phys. **125**, 194522 (2006).
[35] K. Kwak, S. Park, I. J. Finkelstein, and M. D. Fayer, J. Chem. Phys. **127**, 1245031 (2007).
[36] A. Piryatinski and J. L. Skinner, J. Phys. Chem. B **106**, 8055 (2002).
[37] P. Hamm and R. M. Hochstrasser, in *Ultrafast Infrared and Raman Spectroscopy*, edited by M. D. Fayer (Dekker, New York, 2001), Vol. 26, pp. 273–347.
[38] O. Kinrot and Y. Prior, Phys. Rev. A **51**, 4996 (1995).
[39] N. Belabas and D. M. Jonas, J. Opt. Soc. Am. B **22**, 655 (2005).
[40] D. Keusters and W. S. Warren, J. Chem. Phys. **119**, 4478 (2003).
[41] *Ultrafast Infrared and Raman Spectroscopy*, edited by M. D. Fayer (Dekker, New York, 2001), Vol. 26.
[42] K. D. Rector, D. A. Zimdars, and M. D. Fayer, J. Chem. Phys. **109**, 5455 (1998).
[43] R. W. Olson, H. W. H. Lee, F. G. Patterson, and M. D. Fayer, J. Chem. Phys. **76**, 31 (1982).
[44] T. Steinel, J. B. Asbury, S. A. Corcelli, C. P. Lawrence, J. L. Skinner, and M. D. Fayer, Chem. Phys. Lett. **386**, 295 (2004).